Self-assembled lipid and membrane protein polyhedral nanoparticles

Tamara Basta[a,1], Hsin-Jui Wu[b,1], Mary K. Morphew[a], Jonas Lee[c,d], Nilanjan Ghosh[a], Jeffrey Lai[c,d], John M. Heumann[a], Keeshia Wang[c], Y. C. Lee[b], Douglas C. Rees[c,d,2], and Michael H. B. Stowell[a,b,2]

[a]Molecular, Cellular, and Developmental Biology and [b]Mechanical Engineering, University of Colorado at Boulder, Boulder, CO 80309; and [c]Howard Hughes Medical Institute and [d]Division of Chemistry and Chemical Engineering, California Institute of Technology, Pasadena, CA 91125

Contributed by Douglas C. Rees, November 26, 2013 (sent for review January 28, 2012)

We demonstrate that membrane proteins and phospholipids can self-assemble into polyhedral arrangements suitable for structural analysis. Using the *Escherichia coli* mechanosensitive channel of small conductance (MscS) as a model protein, we prepared membrane protein polyhedral nanoparticles (MPPNs) with uniform radii of ∼20 nm. Electron cryotomographic analysis established that these MPPNs contain 24 MscS heptamers related by octahedral symmetry. Subsequent single-particle electron cryomicroscopy yielded a reconstruction at ∼1-nm resolution, revealing a conformation closely resembling the nonconducting state. The generality of this approach has been addressed by the successful preparation of MPPNs for two unrelated proteins, the mechanosensitive channel of large conductance and the connexon Cx26, using a recently devised microfluidics-based free interface diffusion system. MPPNs provide not only a starting point for the structural analysis of membrane proteins in a phospholipid environment, but their closed surfaces should facilitate studies in the presence of physiological transmembrane gradients, in addition to potential applications as drug delivery carriers or as templates for inorganic nanoparticle formation.

membrane protein structure | proteoliposomes | electron microscopy | microfluidic devices

The functions of many membrane proteins are intimately coupled to the generation, utilization, and/or sensing of transmembrane gradients (1). Despite advances in the structure determination of membrane proteins (2), the high-resolution structural analysis of membrane proteins in a biological membrane is uncommon and in the presence of a functionally relevant gradient remains an as-yet unrealized experimental challenge. This stems from the fact that the primary 2D- and 3D ordered specimens used in structural studies of membrane proteins by X-ray crystallography and electron microscopy lack closed membrane surfaces, thus making it impossible to establish physiologically relevant transmembrane gradients.

As an alternative, we have been developing methodologies for the self-assembly of lipids and membrane proteins into closed polyhedral structures that can potentially support transmembrane gradients for structural and functional studies. The possibility of generating polyhedral arrangements of membrane proteins in proteoliposomes was motivated by the existence of polyhedral capsids of membrane-enveloped viruses (3, 4), the ability of surfactant mixtures to self-assemble into polyhedral structures (5, 6), and the formation of proteoliposomes from native membranes containing bacteriorhodopsin (7, 8) and light-harvesting complex II (LHCII) (9). Significantly, the high-resolution structure of LHCII was determined from crystals of icosahedral proteoliposomes composed of protein subunits in chloroplast lipids (10). Whereas detergent solubilized membrane proteins and lipid mixtures can self-assemble to form 2D-ordered crystalline sheets or helical tubes favorable for structure determination by electron microscopy (11–14), simple polyhedral ordered assemblies have only been described to form from select native membranes (7–9). To expand the repertoire of membrane protein structural methods, we have prepared membrane protein polyhedral nanoparticles (MPPNs) of the bacterial mechanosensitive channel of small conductance (MscS) (15, 16) from detergent solubilized protein and phospholipids, and demonstrated that they are amenable to structural analysis using electron microscopy.

Conditions for generating MPPNs were anticipated to resemble those for other types of 2D-ordered bilayer arrangements of membrane proteins, particularly 2D crystals, in that membrane protein is mixed with a particular phospholipid at a defined ratio, followed by dialysis to remove the solubilizing detergent (17). The main distinction is that because MPPNs are polyhedral, conditions are sought that will stabilize highly curved surfaces of polyhedra rather than the planar (flat) specimens desired for 2D crystals. We used the *Escherichia coli* MscS as a model system. MscS is an intrinsically stretch-activated channel identified by Booth and coworkers (15) that confers resistance to osmotic downshock in *E. coli*. MscS forms a heptameric channel with 21 transmembrane helices (3 from each subunit) and a large cytoplasmic domain with overall dimensions of ∼8 × ∼12 nm parallel and perpendicular to the membrane plane; structures have been reported in both nonconducting (16, 18) and open-state conformations (19). Different phospholipids were added to purified the *E. coli* MscS solubilized in the detergent Fos-Choline 14 and the system was allowed to reach equilibrium by dialysis at different temperatures. To gain insight into the biophysical parameters that govern MPPN formation, we investigated the role of lipid head

Significance

An alternate strategy to tubular or 2D crystals for high-resolution membrane protein structure determination by electron microscopy has been developed. Homogeneous polyhedral proteoliposomes of defined symmetry were prepared from the *Escherichia coli* mechanosensitive channel of small conductance (MscS). These membrane protein polyhedral nanoparticles (MPPNs) were analyzed by electron cryomicroscopy that established that they contain 24 MscS heptamers related by octahedral symmetry wherein the individual MscS conformation resembles the nonconducting state. We further demonstrate the development of a membraneless microfluidic device that can facilitate the preparation of a variety of MPPNs, with future applications including structural studies of membrane proteins in the presence of transmembrane gradients, as well as drug delivery carriers or as templates for inorganic nanoparticle formation.

Author contributions: T.B., H.-J.W., M.K.M., Y.C.L., D.C.R., and M.H.B.S. designed research; T.B., H.-J.W., M.K.M., J. Lee, N.G., J. Lai, K.W., D.C.R., and M.H.B.S. performed research; J. Lee, J. Lai, J.M.H., K.W., and Y.C.L. contributed new reagents/analytic tools; T.B., H.-J.W., M.K.M., J. Lee, N.G., J.M.H., Y.C.L., D.C.R., and M.H.B.S. analyzed data; and D.C.R. and M.H.B.S. wrote the paper.

The authors declare no conflict of interest.

[1]T.B. and H.-J.W. contributed equally to this work.

[2]To whom correspondence may be addressed. E-mail: dcrees@caltech.edu or stowellm@colorado.edu.

This article contains supporting information online at www.pnas.org/lookup/suppl/doi:10.1073/pnas.1321936111/-/DCSupplemental.

www.pnas.org/cgi/doi/10.1073/pnas.1321936111

group, alkyl chain length, pH, and protein construct. Table S1 shows the observed influence of these various factors on our ability to form uniform MPPNs (as opposed to disordered aggregates or polydisperse proteoliposomes). The optimal conditions for MPPN formation used 1,2-dimyristoyl-*sn*-glycero-3-phosphocholine [added to ~1:0.1 (wt/wt) protein:phospholipid] at pH 7 with the His-tagged MscS that is anticipated to be positively charged under these conditions. The biophysical properties of the protein are important as the best results were achieved using a His-tagged construct and the presence of a FLAG tag at the C terminus of MscS interfered with MPPN formation, even though the tag is ~10 nm from the membrane-spanning region of MscS.

To monitor MPPN formation, dynamic light scattering (DLS) was used. Under optimal conditions, we observed (Fig. 1*A*) the complete transition of solubilized MscS particles with a narrow distribution centered around a mean radii of 4.5 nm to MPPNs with a narrow distribution centered around a mean radii of 20 nm. We further characterized these particles using negative-stain electron microscopy. Fig. 1*B* is a field view negative-stain electron micrograph of a solution of detergent-solubilized MscS and lipid before initiation of the self-assembly process. Fig. 1*C* is a field view negative-stain electron micrograph of the same sample after the self-assembly process. We observed the incorporation of MscS into highly uniform polyhedra with mean radii of ~20 nm (90%) and ~17 nm (10%) by negative-stain electron microscopy. To gain more insight into the biophysical properties of these particles, we performed protein and phosphorus analysis on multiple samples to determine the lipid:protein ratio (Fig. S1). The observed lipid:protein ratio of the MscS MPPNs was 11 ± 1 (mole lipid:mole protein subunit) and consistent with a single layer of lipids forming a bilayer surrounding each protein. This ratio is comparable to the observed lipid to protein ratio found in 2D crystals of membrane proteins such as bacteriorhodopsin (lipid:protein ratio of 10; refs. 20 and 21) and aquaporin (lipid:protein ratio of 9; ref. 22).

To further elucidate the structural nature of these particles and to unambiguously determine the symmetry, we performed electron cryotomography with image reconstruction using IMOD (23) combined with Particle Estimation for Electron Tomography (PEET) program (ref. 24 and *SI Materials and Methods*). In principle, electron tomography provides a complete 3D map of the particles and would allow us to unambiguously determine the MPPN symmetry. However, the alignment process was highly biased by the missing wedge phenomenon (24) due to poor signal: noise and resulted in an incomplete map (Fig. 2*A*). To overcome this alignment bias, we assigned random initial orientation values to all particles and constrained possible angular shifts to less than 30° to achieve a more uniform distribution of orientations (Fig. S2). This strategy resulted in a much improved density map (Fig. 2*B*) that revealed individual molecules with a size and shape that are in good agreement to the known molecular structure of MscS (Fig. 2*C* and Fig. S3). Building on the analysis of Haselwandter and Phillips (25), a systematic analysis was conducted (Table S2) of the symmetry relationships between MscSs in MPPNs that identified the arrangement corresponding to the snub cuboctahedron (dextro), an Archimedean solid. The snub cuboctahedron has cubic (octahedral) symmetry which, as recognized by Crick and Watson (26), provides an efficient way to pack identical particles in a closed, convex shell. In this particular arrangement, 24 MscS molecules are related by the 432-point group symmetry axes that pass through the faces, but not the vertices, of the snub cuboctahedron. Because the MscS molecules are positioned on the vertices of this chiral polyhedron, they occupy general positions that permit the ordered packing of the heptamers of a biomacromolecule (or indeed any type of particle). This is an important observation as it means that the individual MscS molecules with sevenfold symmetry are capable of packing into a symmetric assembly that is amenable to averaging. Whereas 24 objects can be arranged with identical environments in a snub cuboctahedron, certain integer multiples of this number can also be accommodated using the principles of quasiequivalence (27, 28) to form larger closed shells.

Using the symmetry derived by electron cryotomography, we proceeded to collect high-resolution single-particle electron cryomicroscopy data. Samples prepared identically for cryotomography were imaged under low-dose conditions and a total of 4,564 particles were processed using the Electron Micrograph Analysis 2 (EMAN2) software package (*SI Materials and Methods*) (29). The final map had a resolution of 9 Å by Fourier shell correlation (Fig. S4) and allowed us to model the inner and outer helices of the transmembrane pore (Fig. 3). The arrangement of the helices more closely resembles the nonconducting conformation (16, 18) than the open-state structure (19), although some differences in the positioning of the outer helices relative to the nonconducting

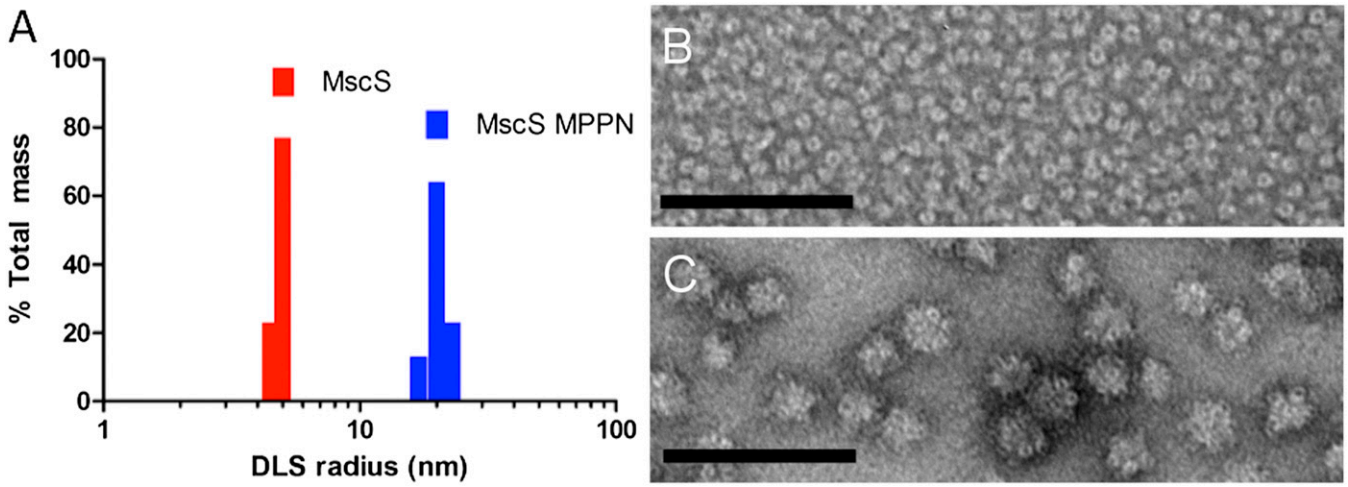

Fig. 1. Preparation of MscS MPPNs. (*A*) DLS analysis of particles before dialysis and after completion of dialysis when MPPNs are formed. The observed radius of MscS alone was 4.5 nm and the particle radius at the end of dialysis was observed to be 20 nm. In both cases 99% of the scattering mass was observed in the distributions centered at 4.5 nm and 20 nm, respectively. (*B*) Negative-stain electron microscopy analysis of MscS before dialysis. Individual MscS proteins can be observed as small doughnut-shaped particles. (*C*) Negative-stain electron microscopy analysis of MPPNs following dialysis of the sample in *B*. MPPNs can be clearly observed and appear as uniform assemblies of individual MscS molecules. (Scale bars, 100 nm.)

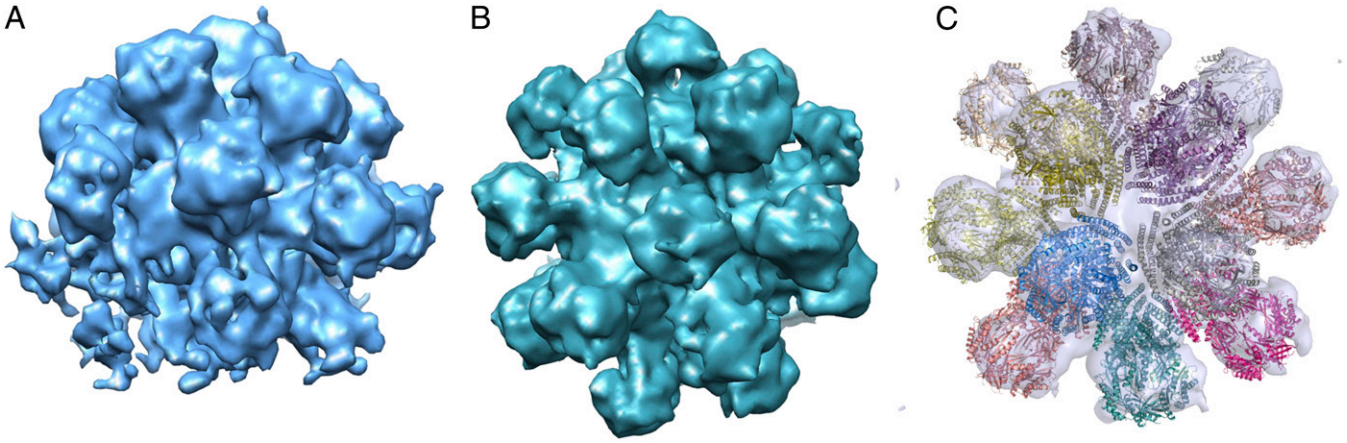

Fig. 2. Cryotomography of MscS MPPNs. (*A*) The PEET isosurface derived from 162 individual particles selected from eight single-tilt tomograms. The strong bias due to the missing wedge is observed along the lower part of the surface, but individual MscS heptamers are still discernible in the image. (*B*) The corresponding PEET isosurface, following introduction of randomized starting Euler angles to minimize missing-wedge bias. (*C*) The use of randomized starting Euler angles results in a much-improved map with apparent octahedral (432) symmetry that could be fit with 24 molecules of the MscS crystal structure. Isosurface renderings of the volume averages were generated using Chimera (31).

structure are indicated in sections 2 and 3 of Fig. 3. These results demonstrate that membrane proteins are capable of assembling into MPPNs that are amenable to high-resolution structure analysis by single-particle electron cryomicroscopy. Higher resolution data will be required, however, to detail the precise conformational differences between MscS in the phospholipid environment of MPPNs compared with those in the detergent-solubilized state used in the X-ray crystal structure analyses.

In these promising initial studies we used traditional dialysis methods to screen conditions for MPPN formation. These methods are time consuming and require substantial quantities of a sample. To more efficiently screen conditions for MPPN formation with a variety of membrane proteins, we designed and fabricated a free interface diffusion microfluidic device (30) (Fig. 4*A* and Fig. S5) This device greatly simplifies the screening process and minimizes the amount of sample required for determining suitable conditions for MPPN formation. Using this device, we were able to produce MPPNs from MscS but more importantly from several other proteins that had previously failed to produce MPPNs using traditional dialysis. Fig. 4 *B* and *C* shows the results of using this device for the mechanosensitive channel of large conductance (MscL) and

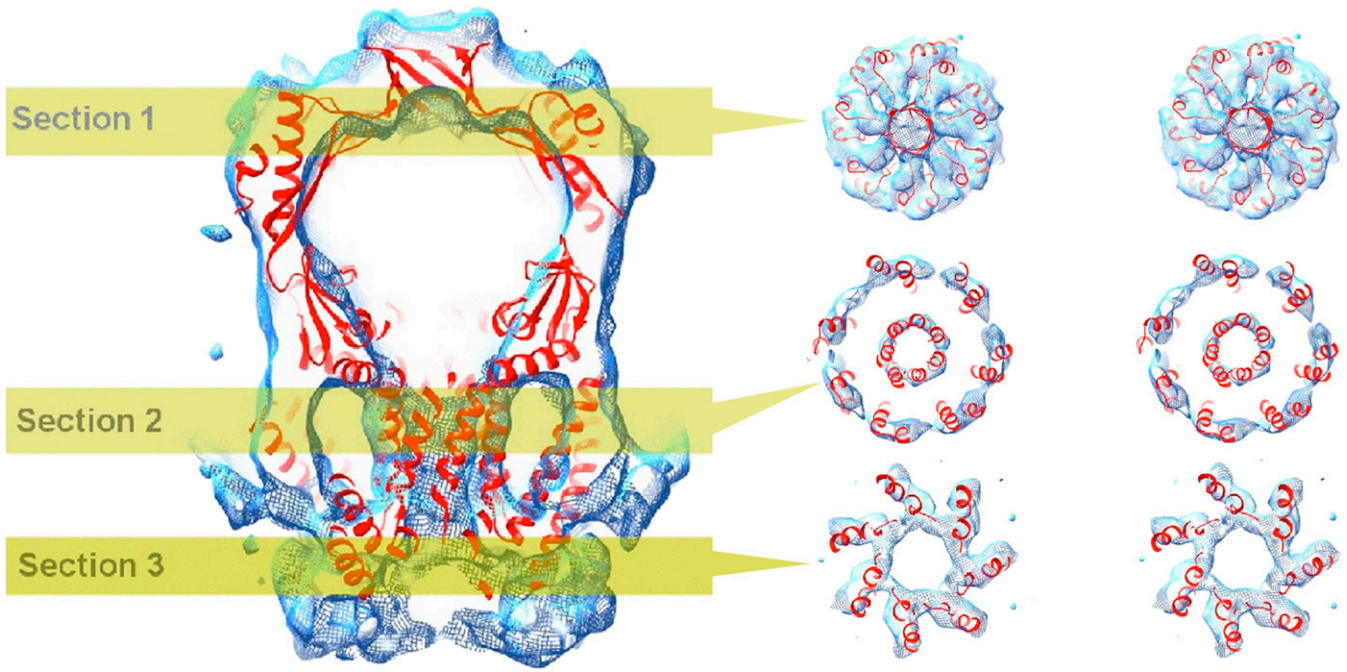

Fig. 3. Single-particle image analysis reconstructed from 4,564 particles processed with EMAN2 and subsequently the density surrounding a single MscS heptamer was extracted and sevenfold averaged as described in *SI Materials and Methods*. (*Left*) A cross-section through the electron density revealing the translocation pathway and cytoplasmic vestibule, and showing the overall fit of the closed structure of MscS (red ribbons) fit to the map (cyan). (*Right*) Stereoviews of cross-sections in the density map normal to the sevenfold axis at sections 1, 2, and 3. The closed-structure coordinates (red ribbons) of MscS were fit to the map using rigid body refinement in Chimera (31) showing the position of the transmembrane helices.

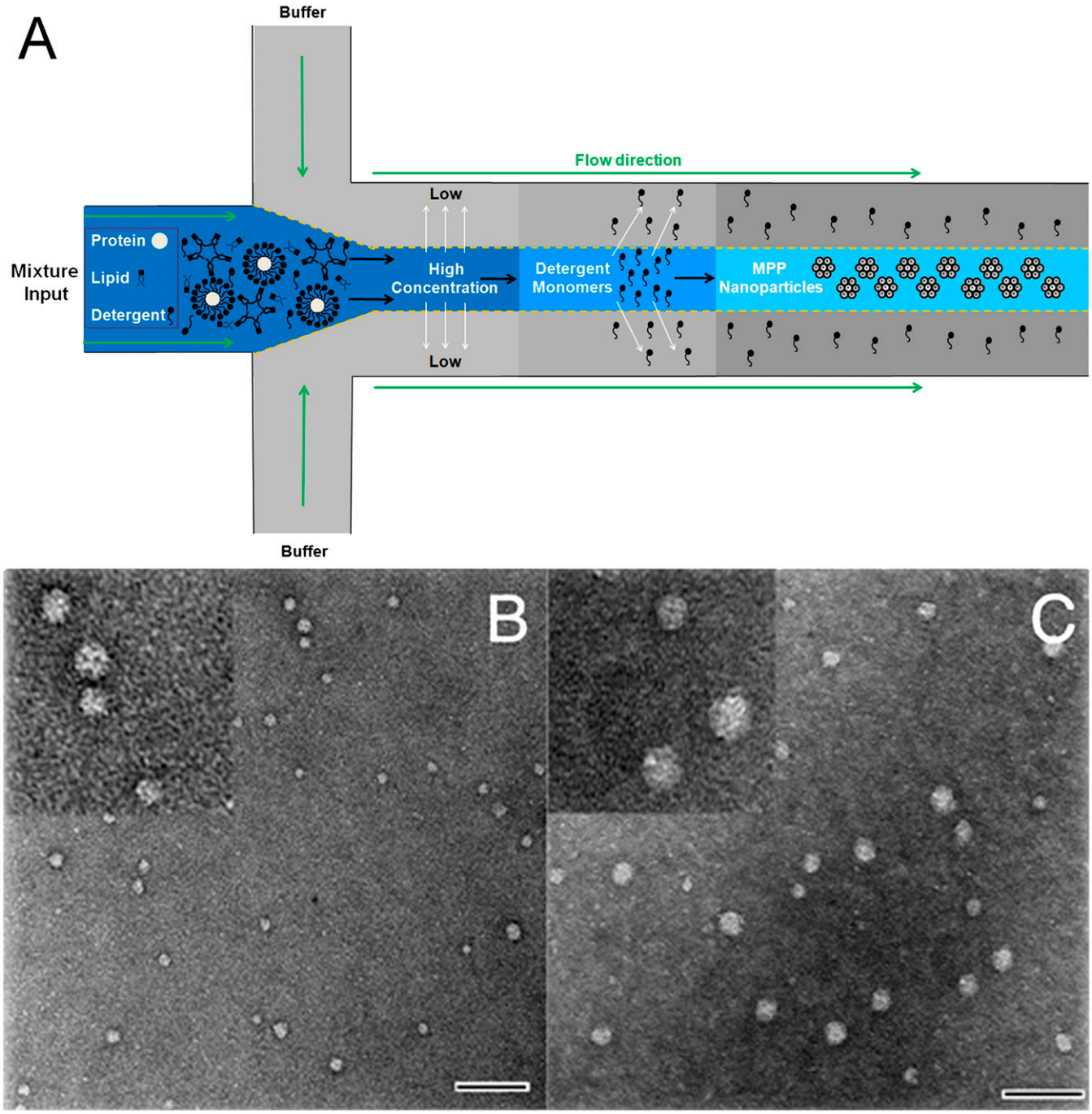

Fig. 4. Preparation of MPPNs using a microfluidics-based free interface diffusion system. (*A*) Schematic illustration of the device used for lipid–protein nanoparticle formation. From left to right, molecules in the center flow diffuse into the outer flow by the concentration gradient, with small molecules (larger diffusion coefficient) moving more quickly than larger molecules. Specifically, monomer detergents are removed through interfacial diffusion, whereas larger membrane proteins remain in the center flow, forming nanoparticles. Both the ratio of input:buffer and the flow rate influence particle formation. (*B*). Negative-stain electron microscopy images of MPPNs of MscL and (*C*) Cx26 formed using the microfluidic device from *A*. (Scale bar, 100 nm.) *Insets* show 2.5× magnification of a select region of interest.

the connexon Cx26, respectively, where polyhedra were only observed in the presence of the target protein. Intriguingly, several different particles sizes could be observed for both MscL and Cx26 and we hypothesize that the variable-sized polyhedra may correspond to different packing arrangements similar to triangulation numbers observed in viral polyhedral assemblies. This microfluidic device will provide rapid screening of conditions for the formation of MPPNs and it is hoped will expedite membrane protein structural analysis in native lipid environments.

The self-assembly of membrane proteins into polyhedral nanoparticles demonstrates a potentially powerful method for studying the structure and function of membrane proteins in a lipid environment. MPPNs represent a novel form of lipid–protein assemblies which lie between single particles and large crystalline sheets or tubes. We have demonstrated that conditions

favorable for MPPN formation can be identified and have elucidated the structure, symmetry, and potential application to membrane protein structure analysis. In addition we have designed and fabricated microfluidic devices for high-throughput screening of conditions for MPPN formation. MPPNs may allow a variety of perturbations to be achieved such as pH, voltage, osmotic, concentration gradients, etc. that cannot be achieved with other membrane protein assemblies and will potentially allow us to activate various types of gated channels and receptors so that active conformational states can be structurally investigated. The potential of such materials for targeted drug delivery with precisely controlled release mechanisms offers an intriguing avenue for future biomedical applications.

Materials and Methods

MPPNs were prepared from purified *E. coli* MscS (16) solubilized in the detergent Fos-Choline 14 by dialysis in the presence of phospholipids. The best results were obtained using the His-tagged MscS and phosphatidylcholine with a saturated 14 carbon containing fatty acid alkyl chain dialyzed at pH 7. MPPNs were characterized by negative-stain electron microscopy, electron cryotomography, and single-particle electron cryomicroscopy. The octahedral symmetry of the MPPNs was established by analysis of the relative positions of MscS heptamers manually docked in the tomograms reconstructed with PEET (24). The symmetry derived by electron cryotomography was subsequently used to process single-particle electron cryomicroscopy using EMAN2 software (29). Details of these procedures are provided in *SI Materials and Methods*.

ACKNOWLEDGMENTS. We thank our colleagues at the University of Colorado and California Institute of Technology (Caltech) for helpful comments and criticisms, Randal Bass (Caltech) for providing initial MscS samples, Mark Yeager and Brad Bennett (University of Virginia) for providing samples of Cx26, Steven Ludtke (Baylor University) for EMAN advice, Rob Phillips and Christoph Haselwandter (Caltech) for discussions on polyhedral symmetry, and Chris Arthur (Oregon Health and Science University) and Axel Brilot (Brandeis University) for assistance with image scanning. Molecular graphics images were produced using the University of California, San Francisco (UCSF) Chimera package from the Resource for Biocomputing, Visualization, and Informatics at UCSF (supported by NIH-P41RR001081). Electron microscopy was performed in the Laboratory for 3D Electron Microscopy of Cells at the University of Colorado (supported by NIH-P41GM103431-42). This work was supported in part by a National Institutes of Health (NIH) Exceptional, Unconventional Research Enabling Knowledge Acceleration (EUREKA) Award (to M.H.B.S.), a Howard Hughes Medical Institute Collaborative Innovation Award (to D.C.R. and M.H.B.S.), and NIH Grant GM084211 (to D.C.R.).

1. Nicholls DG, Ferguson SJ (2002) *Bioenergetics 3* (Academic, London), p 297.
2. White SH (2004) The progress of membrane protein structure determination. *Protein Sci* 13(7):1948–1949.
3. Zhang W, et al. (2003) Visualization of membrane protein domains by cryo-electron microscopy of dengue virus. *Nat Struct Biol* 10(11):907–912.
4. Cockburn JJB, et al. (2004) Membrane structure and interactions with protein and DNA in bacteriophage PRD1. *Nature* 432(7013):122–125.
5. Dubois M, et al. (2001) Self-assembly of regular hollow icosahedra in salt-free catanionic solutions. *Nature* 411(6838):672–675.
6. Dubois M, et al. (2004) Shape control through molecular segregation in giant surfactant aggregates. *Proc Natl Acad Sci USA* 101(42):15082–15087.
7. Takeda K, et al. (1998) A novel three-dimensional crystal of bacteriorhodopsin obtained by successive fusion of the vesicular assemblies. *J Mol Biol* 283(2):463–474.
8. Denkov ND, Yoshimura H, Kouyama T, Walz J, Nagayama K (1998) Electron cryomicroscopy of bacteriorhodopsin vesicles: Mechanism of vesicle formation. *Biophys J* 74(3):1409–1420.
9. Hino T, Kanamori E, Shen JR, Kouyama T (2004) An icosahedral assembly of the light-harvesting chlorophyll a/b protein complex from pea chloroplast thylakoid membranes. *Acta Crystallogr D Biol Crystallogr* 60(Pt 5):803–809.
10. Liu Z, et al. (2004) Crystal structure of spinach major light-harvesting complex at 2.72 A resolution. *Nature* 428(6980):287–292.
11. Stowell MH, Miyazawa A, Unwin N (1998) Macromolecular structure determination by electron microscopy: New advances and recent results. *Curr Opin Struct Biol* 8(5):595–600.
12. Glaeser RM, Downing K, DeRosier D, Chiu W, Frank J (2007) *Electron Crystallography of Biological Molecules* (Oxford Univ Press, Oxford).
13. Raunser S, Walz T (2009) Electron crystallography as a technique to study the structures of membrane proteins in a lipid environment. *Ann. Rev. Biophys.* 38:89–105.
14. Fujiyoshi Y (2011) Structural physiology based on electron crystallography. *Protein Sci* 20(5):806–817.
15. Levina N, et al. (1999) Protection of *Escherichia coli* cells against extreme turgor by activation of MscS and MscL mechanosensitive channels: Identification of genes required for MscS activity. *EMBO J* 18(7):1730–1737.
16. Bass RB, Strop P, Barclay M, Rees DC (2002) Crystal structure of *Escherichia coli* MscS, a voltage-modulated and mechanosensitive channel. *Science* 298(5598):1582–1587.
17. Schmidt-Krey I (2007) Electron crystallography of membrane proteins: Two-dimensional crystallization and screening by electron microscopy. *Methods* 41(4):417–426.
18. Steinbacher S, Bass RB, Strop P, Rees DC (2007) Structures of the prokaryotic mechanosensitive channels MscL and MscS. *Curr Topics Membranes* 58:1–24.
19. Wang WJ, et al. (2008) The structure of an open form of an *E. coli* mechanosensitive channel at 3.45 A resolution. *Science* 321(5893):1179–1183.
20. Mitsuoka K, et al. (1999) The structure of bacteriorhodopsin at 3.0 A resolution based on electron crystallography: Implication of the charge distribution. *J Mol Biol* 286(3):861–882.
21. Grigorieff N, Ceska TA, Downing KH, Baldwin JM, Henderson R (1996) Electron-crystallographic refinement of the structure of bacteriorhodopsin. *J Mol Biol* 259(3):393–421.
22. Gonen T, et al. (2005) Lipid-protein interactions in double-layered two-dimensional AQP0 crystals. *Nature* 438(7068):633–638.
23. Kremer JR, Mastronarde DN, McIntosh JR (1996) Computer visualization of three-dimensional image data using IMOD. *J Struct Biol* 116(1):71–76.
24. Nicastro D, et al. (2006) The molecular architecture of axonemes revealed by cryoelectron tomography. *Science* 313(5789):944–948.
25. Haselwandter CA, Phillips R (2010) Minimal bending energies of bilayer polyhedra. *Phys Rev Lett* 105(22):228101.
26. Crick FHC, Watson JD (1956) Structure of small viruses. *Nature* 177(4506):473–475.
27. Caspar DL, Klug A (1962) Physical principles in the construction of regular viruses. *Cold Spring Harb Symp Quant Biol* 27:1–24.
28. Plevka P, Tars K, Liljas L (2008) Crystal packing of a bacteriophage MS2 coat protein mutant corresponds to octahedral particles. *Protein Sci* 17(10):1731–1739.
29. Ludtke SJ, Baldwin PR, Chiu W (1999) EMAN: Semiautomated software for high-resolution single-particle reconstructions. *J Struct Biol* 128(1):82–97.
30. Wu H-J, et al. (2013) Microfluidic device for super-fast evaluation of membrane protein nanoparticle formation. *Micro & Nano Letters* 8(10):672–675.
31. Pettersen EF, et al. (2004) UCSF Chimera—a visualization system for exploratory research and analysis. *J Comput Chem* 25(13):1605–1612.